

GDPS-User Manual

V1.0

Software: GNSS Data Preprocessing Software (GDPS)

Developer: Liguo Lu

Address: School of Surveying and Geoinformation Engineering, East China University of Technology, Nanchang 330013, China

E-mail: lglu66@163.com

April 2024

Content

1 Overview	1
2 Software requirements.....	2
2.1 Environmental requirements	2
2.2 Software license.....	2
3 Software installation	3
4 Software and tools instructions.....	5
4.1 Format translation	5
4.2 Data editing	6
4.3 Quality checking	7
4.4 Auxiliary tools.....	7
5 Software operation	9
5.1 Format translation operation	9
5.2 Data editing operation.....	9
5.3 Quality checking operation	9
6 Mathematical methods	16
6.1 Pseudorange gross error detection	16
6.2 Cycle slip detection.....	16
6.2.1 MW combination	16
6.2.2 GF combination	17
6.3 Clock jump detection and repair	17
6.4 Data integrity rate	18
6.5 Data saturation rate	18
6.6 Pseudorange multipath.....	18
6.7 Carrier phase multipath.....	19
6.8 Ionospheric delay rate	19
6.9 Carrier-to-noise ratio.....	19
6.10 Pseudorange observation noise	19
6.11 Carrier phase observation noise	19
6.12 Dilution of precision	20
Acknowledgement	21

1 Overview

With the rapid development of multi-frequency and multi-system GNSS, users can access a wealth of observation data from navigation systems like BeiDou Satellite Navigation System (BDS), Global Positioning System (GPS), Global Navigation Satellite System (GLONASS), and Galileo satellite navigation system (Galileo), etc. However, the quality of these original GNSS observations is easily affected by signal availability, transmission errors, multipath, and receiver performance. GNSS data preprocessing is a prerequisite for high-precision GNSS navigation, positioning, and orbit determination applications. While commercial software toolboxes are available, these existing preprocessing tools are not user-friendly enough to handle multi-frequency and multi-system GNSS data due to extra costs, strong professionalism, and complex operations. Therefore, we propose an open-source GNSS data preprocessing software (GDPS) developed in Python, which supports compiling and running under operating systems such as Windows and Linux.

The main features of this software are as follows:

- ✧ GDPS provides an open-source Python-based interactive tool on Windows and Linux to preprocess multi-frequency and multi-system GNSS data, such as GPS, GLONASS, Galileo, BDS, QZSS, IRNSS, and SBAS.
- ✧ GDPS supports format translation on different versions of RINEX 2.11~4.01 data files, such as observation data, broadcast ephemerides, and meteorological data.
- ✧ GDPS supports editing processing based on RINEX data, including data segmentation, splicing, and extraction modules, to modify the required data record contents.
- ✧ GDPS supports quality checking analysis of multi-GNSS data in terms of carrier-to-noise-density ratio, ionospheric delay rate, pseudorange/carrier phase multipath, pseudorange/carrier phase observation noise, data integrity/saturation rate, and single point positioning.

2 Software requirements

2.1 Environmental requirements

The executable program in the package is built by Pycharm 2019 and Python 3.7 with open-source, cross-platform compilation tools on Windows 10. Computer configuration requirements are as follows:

Operating systems: Windows or Linux

System type: 64-bit

Memory: at least 512MB

Hard disk space: at least 500MB

2.2 Software license

GDPS is an open-source software governed by the GNU General Public License (version 3) (<https://www.gnu.org/licenses/gpl-3.0.html>). Users can redistribute or modify it under the terms of the GNU General Public License published by the Free Software Foundation.

3 Software installation

After downloading the GDPS package and ensuring the necessary tools (such as Python 3.7 and Pycharm 2019) are available, please follow the steps below to compile the software.

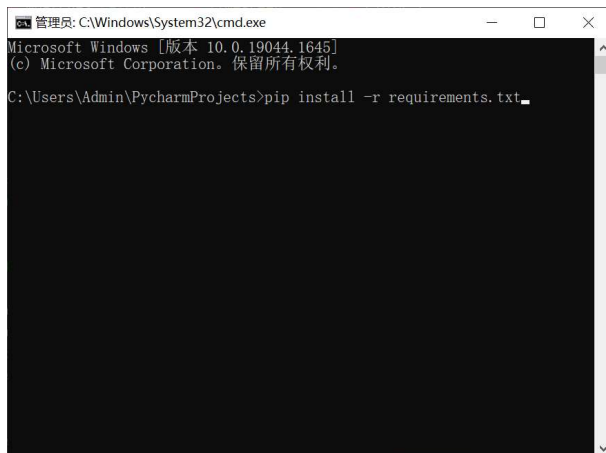
Step 1: Uncompress the GDPS.zip file, then get three folders (i.e. \data, \doc, and \src). "\src" represents the source code and its directory structure is shown in Fig. 1.

> config_format	GUI_Edit_CombData.py
> data_edit	GUI_Edit_CutData.py
> format_convert	GUI_Edit_ExtraData.py
> images	GUI_Help.py
> lib	GUI_Quality_Check_plotsat.py
> map	GUI_Quality_Check_plotsys.py
> plot	GUI_Quality_Check_setup.py
> quality_check	GUI_Quality_Check.py
> tables	GUI_tableview.py
> tool	GUI_Tool_CoorConv.py
> tutorial	GUI_Tool_TimeConv.py
GDPS.log	LICENSE
GDPS.py	loger.py
get_station_list.py	pyinstaller.txt
global_var.py	read_sol.py
GUI_Conversion_Met.py	README.md
GUI_Conversion_Nav.py	requirements.txt
GUI_Conversion_Obs.py	resources_rc.py
	resources.qrc

Fig. 1 "\src" folder directory structure

Step 2: Execute the installation command (pip install -r requirements.txt) through the console.

Fig. 2 shows the input in the Windows environment.



The screenshot shows a Windows Command Prompt window titled "管理员: C:\Windows\System32\cmd.exe". The window displays the following text:
Microsoft Windows [版本 10.0.19044.1645]
(c) Microsoft Corporation。保留所有权利。
C:\Users\Admin\PycharmProjects>pip install -r requirements.txt

Fig. 2 Installation package list

Step 3: Create a project in Pycharm and run GDPS.py. Fig. 3 displays the software interface.



Fig. 3 GDPS main interface

4 Software and tools instructions

GDPS software mainly includes four functional modules: format translation, data editing, quality checking, and auxiliary tools, as shown in Fig.4.

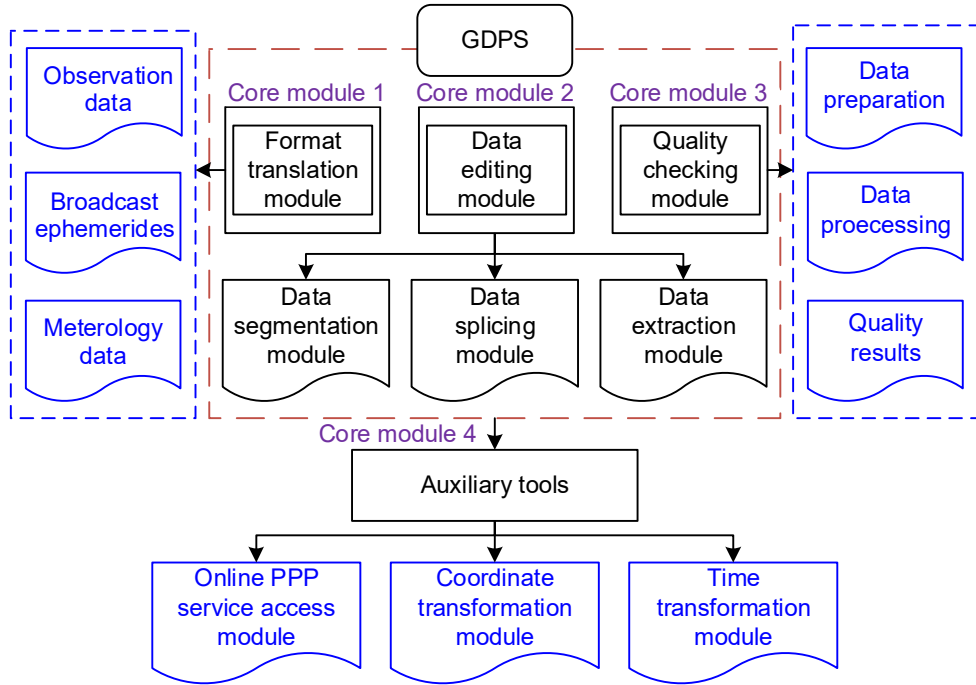


Fig. 4 Software functional modules

4.1 Format translation

The format translation module realizes the conversion of GNSS data between RINEX 2.11 and 4.01 versions. According to the file type classification, this module deals with observation data, ephemerides, and meteorological data. Users import the input file, select the corresponding RINEX version, and set the output path. Finally, click "Execute" to execute the conversion task.

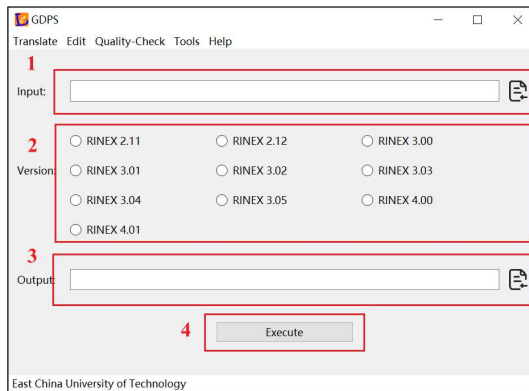


Fig. 5 Format translation module interface

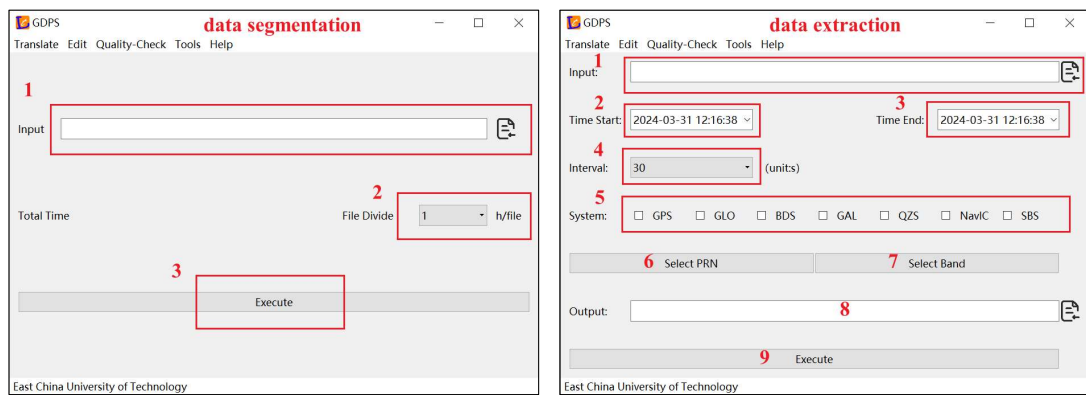
Due to differences in observation code among different versions of RINEX, it is necessary first to determine the priority of observation encoding. Table 1 shows the priority relationship of the observation code for GDPS software.

Table 1 Priority relationship of observation code

System	Band	Type	priority order
GPS	L1	C	C S L X
		P	P W Y M
		L / D / S	P W C S L X Y M N
		C	C D S L X
		P	P W Y M
	L2	L / D / S	P W C D S L X Y M N
		C / L / D / S	I Q X
	G1	C	C
		P	P
		L / D / S	P C
		C	C
		P	P
GLONASS	G2	L / D / S	P C
		C / L / D / S	I Q X
		C / L / D / S	B C X Z A
	G3	C / L / D / S	I Q X
		C / L / D / S	I Q X
	E1	C / L / D / S	B C X Z A
	E5a	C / L / D / S	I Q X
Galileo	E5b	C / L / D / S	I Q X
	E5(E5a+E5b)	C / L / D / S	I Q X
	E6	C / L / D / S	B C X Z A
	B1	C / L / D / S	I Q X
	E5(E5a+E5b)	C / L / D / S	I Q X
BDS	B2/B2b	C / L / D / S	I Q X D P Z
	B3/B3A	C / L / D / S	I Q X D P Z
SBAS	L1	C / L / D / S	C
	L5	C / L / D / S	I Q X

4.2 Data editing

Due to the specific needs of different users, some data record contents need to be modified. The data editing module is concerned with data segmentation, splicing, and extraction to assist users in editing the file structure of observation data. Among them, data splitting is to cut the data of the whole observation period into several periods; data extraction is to access observation values according to the information of frequency code, satellite system, pseudo-random code, sampling interval, and observation duration; and data splicing is to merge several periods into one data.



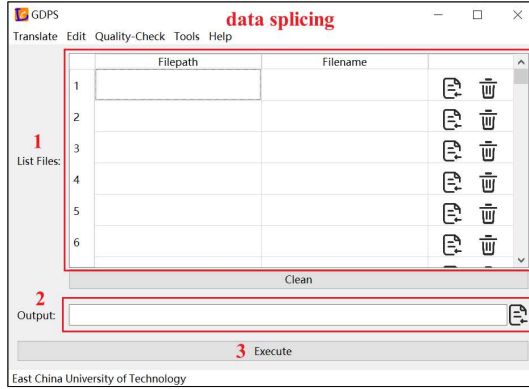


Fig. 6 Data editing module interface

4.3 Quality checking

The quality of observation data is the guarantee of subsequent high-quality positioning services. The quality checking module aims to achieve the calculation and visual analysis of the observation data quality checking indexes. The quality checking results include summary information, carrier-to-noise ratio, ionospheric delay rate, pseudorange/carrier phase multipath, pseudorange/carrier phase noise, data integrity/saturation rate, and single point positioning.

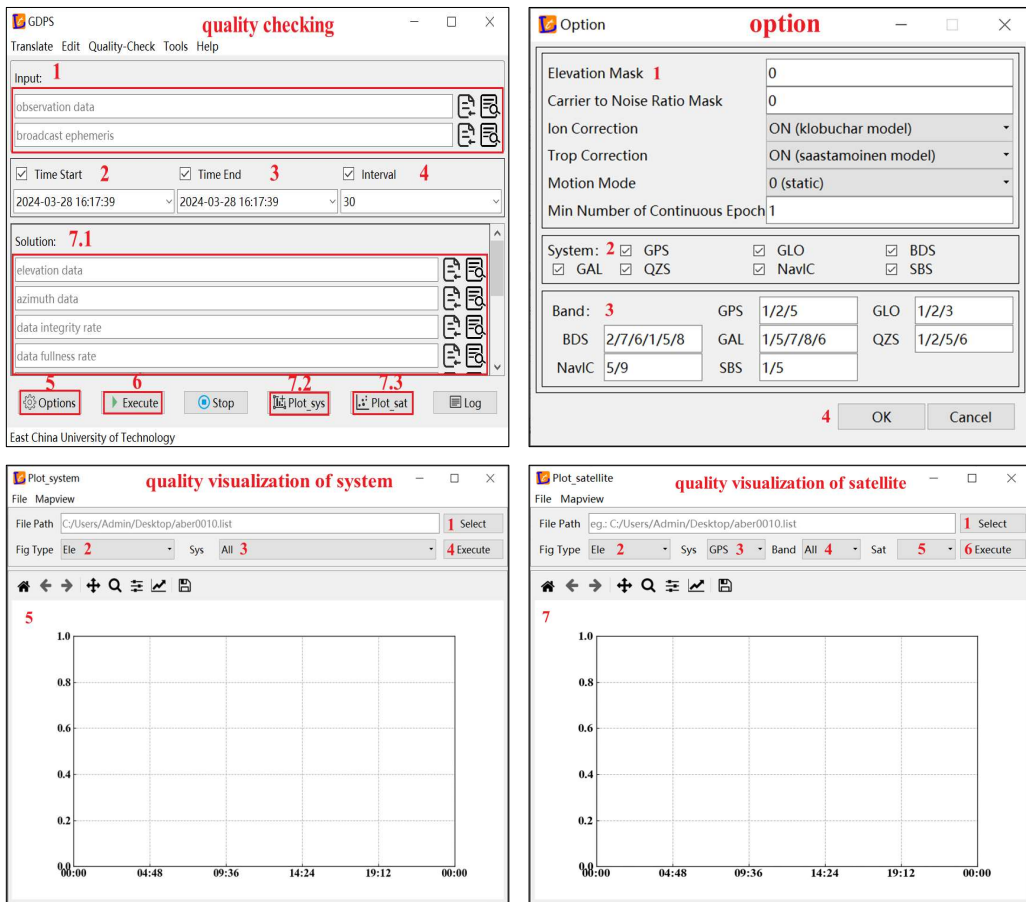


Fig. 7 Quality checking module interface

4.4 Auxiliary tools

GDPS provides some auxiliary tools to improve the efficiency of data processing and

result analysis. The auxiliary tool module mainly includes functions such as PPP service, coordinate transformation, and time transformation. The PPP service module provides several popular online PPP service interfaces, such as APPS, AUSPOS, CSRS-PPP, GAPS, magicGNSS, Net _ Diff, OPUS, and RTX-PP. The coordinate transformation module supports coordinate transformation between XYZ, NEU, and BLH in batch processing mode. The time transformation module provides the conversion function of the year/month/day/minute/second format to the Julian day, simplified Julian day, Day of Year (DOY), GPS week day and week second, and BDS week day and week second.

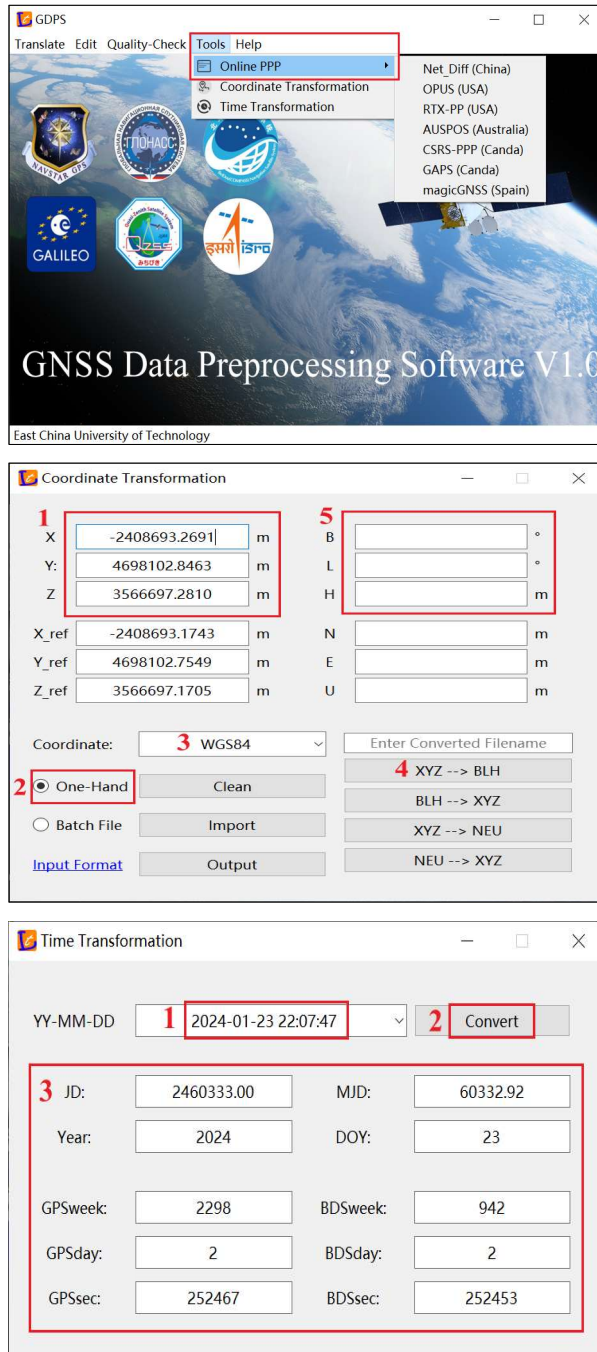


Fig. 8 Auxiliary tools module interface

5 Software operation

5.1 Format translation operation

In the format translation module, users can convert the corresponding version from 3.05 to 2.11, convert the satellite system from multi-GNSS to GPS, GLONASS, Galileo, and SBAS systems, and convert the observation encoding type from a separate system to an integrated encoding.

3.05		OBSERVATION DATA M (MIXED)		RINEX VERSION / TYPE	
JPFGRNX v.3.1.216		JAVAD GNSS		20231104 001547 UTC PGM / RUN BY / DATE	
gfzrnx-3615		FILE PROCESSING		20231104 001723 UTC COMMENT	
WUH200CHN		COMMENT			
21602M007		MARKER NAME			
gnss@gfz-potsdam.de		WHU/GFZ		MARKER NUMBER	
1480954		JAVAD TRE_3		OBSERVER / AGENCY	
3354C		4.2.01+b0-211122		REC # / TYPE / VERS	
0.1206		0.0000		ANTENNA: DELTA H/E/N	
-2267749.0000		5009154.0000		APPROX POSITION XYZ	
P 24 C10 C11 C12 L11 L12 D11 D12 S11 S12 C21 C22		S13 S14 C23 C24 S21 S22 C31 C32		SYS # / TYPES	
C 22 C12 L21 L22 D21 D22 S21 S22 C5X L5X D5X S5X		S5X		SYS # / TYPES	
B 20 C10 C11 C12 L11 L12 D11 D12 S11 S12 C21 C22		C23 C24 S21 S22 C31 C32		SYS # / TYPES	
D22 S22 S23 C3X L3X D3X S3X		S3X		SYS # / TYPES	
E 20 C11 C12 L11 L12 D11 D12 S11 S12 C21 C22		C23 C24 S21 S22 C31 C32		SYS # / TYPES	
L7X D7X S7X C8X L8X D8X S8X		S7X		SYS # / TYPES	
J 16 C10 C11 C12 L11 L12 D11 D12 S11 S12 C21 C22		C23 C24 S21 S22 C31 C32		SYS # / TYPES	
L5X D5X S5X		S5X		SYS # / TYPES	
C 32 C10 C11 C12 L11 C21 L21 D21 S21 C5X L5X D5X S5X		C6X		SYS # / TYPES	
L6X D6X S6X C7D C7J L7D L7T L7E D7D D7T D7B STD		S7X		SYS # / TYPES	
S71 S72 C8X L8X D8X S8X		S8X		SYS # / TYPES	
S 4 C10 C11 C12 SIC		SIC		SYS # / TYPES	
C 4 CSA L5A D5A S5A		S5A		SYS # / TYPES	
R01 1 R02 -4 R07 5 R08 6 R09 -2 R10 -7 R11 0 R17 4		R18		GLONASS SLOT / FRQ #	
R22 -3 R23 3 R24 2 R26 25		R27		GLONASS SLOT / FRQ #	
C1C 0.0000 C1P 0.0000 C2C 0.0000 C2P 0.0000		C3C		GLONASS COD/PBS/BIS	
18		LEAP SECONDS		INTERVAL	
2023 11 4 0 0 0.0000000		0.0000000		TIME OF FIRST OBS	
2023 11 4 1 59 59.0000000		59.0000000		TIME OF LAST OBS	
C01		MARKER TYPE		END OF HEADER	
C02					
> 2023 11 04 00 00 0.0000000 0 64		0.000146410662			
		37341800.779			
		37587642.563			
		36865219.665			

3.05		OBSERVATION DATA M (MIXED)		RINEX VERSION / TYPE	
JPFGRNX v.2.1.216		JAVAD GNSS		20231104 001547 UTC PGM / RUN BY / DATE	
gfzrnx-3615		FILE PROCESSING		20231104 001723 UTC COMMENT	
WUH200CHN		COMMENT			
21602M007		MARKER NAME			
gnss@gfz-potsdam.de		WHU/GFZ			
1480954		JAVAD TRE_3		MARKER NUMBER	
3354C		4.2.01+b0-211122		OBSERVER / AGENCY	
0.1206		0.0000		REC # / TYPE / VERS	
-2267749.0000		5009154.0000		ANTENNA: DELTA H/E/N	
P 24 C10 C11 C12 L11 L12 D11 D12 S11 S12 C21 C22		S13 S14 C23 C24 S21 S22 C31 C32		APPROX POSITION XYZ	
C 22 C12 L21 L22 D21 D22 S21 S22 C31 C32		S3X		SYS # / TYPES	
B 20 C10 C11 C12 L11 L12 D11 D12 S11 S12 C21 C22		C23 C24 S21 S22 C31 C32		SYS # / TYPES	
D22 S22 S23 C3X L3X D3X S3X		S3X		SYS # / TYPES	
E 20 C11 C12 L11 L12 D11 D12 S11 S12 C21 C22		C23 C24 S21 S22 C31 C32		SYS # / TYPES	
L7X D7X S7X C8X L8X D8X S8X		S7X		SYS # / TYPES	
J 16 C10 C11 C12 L11 L12 D11 D12 S11 S12 C21 C22		C23 C24 S21 S22 C31 C32		SYS # / TYPES	
L5X D5X S5X		S5X		SYS # / TYPES	
C 32 C10 C11 C12 L11 C21 L21 D21 S21 C5X L5X D5X S5X		C6X		SYS # / TYPES	
L6X D6X S6X C7D C7J L7D L7T L7E D7D D7B STD		S7X		SYS # / TYPES	
S71 S72 C8X L8X D8X S8X		S8X		SYS # / TYPES	
S 4 C10 C11 C12 SIC		SIC		SYS # / TYPES	
C01		SIC		GLONASS SLOT / FRQ #	
C02		0.0000 C1P 0.0000 C2C 0.0000 C2P 0.0000		GLONASS COD/PBS/BIS	
18		LEAP SECONDS		INTERVAL	
2023 11 4 0 0 0.0000000		0.0000000		TIME OF FIRST OBS	
2023 11 4 1 59 59.0000000		59.0000000		TIME OF LAST OBS	
C01		MARKER TYPE		END OF HEADER	
C02					

Fig. 9 Format translation demonstration

5.2 Data editing operation

In the data editing module, users need to batch import multiple sets of observation data to be merged and then click the "Execute" button to perform data merging.

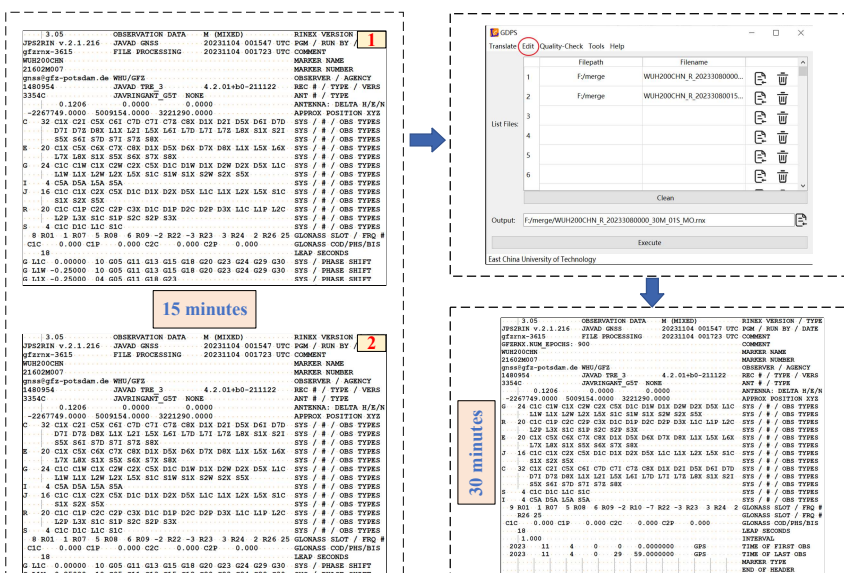


Fig. 10 Data editing demonstration

5.3 Quality checking operation

After importing observation data, broadcast ephemerides, and setting parameters, the

software automatically generates a configuration file to start quality inspection calculation. The output results include summary information, carrier-to-noise ratio, ionospheric delay rate, pseudorange/carrier phase multipath, pseudorange/carrier phase noise, data integrity/saturation rate, and single point positioning.

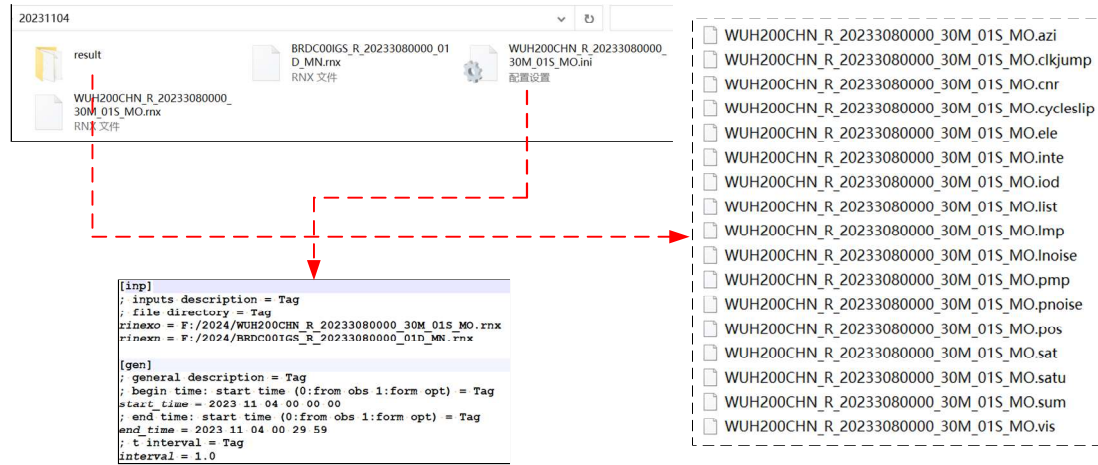


Fig. 11 Quality checking demonstration

Table 2 Output file types

File suffix name	File type
azi	azimuth
ele	elevation
pnoise	pseudorange noise
lnoise	carrier phase noise
cycleslip	cycle slip marker
clkjump	clock jump marker
inte	data integrity rate
satu	data saturation rate
cnr	carrier-to-noise-density ratio
iod	ionospheric delay rate
pmp	pseudorange multipath
lmp	carrier phase multipath
vis	visible satellite markers
pos	single point positioning
list	output file list
sat	satellite list
sum	summary information

GNSS	Date	Time	X (m)	Y (m)	Z (m)	B(deg)	L(deg)	H (m)	Q	NS	GDOP	PDOP	HDOP	VDDP
GPS	2023-11-04	00:00:00	-2267749.48417	5009153.54896	3221293.26178	30.5317	114.3573	26.6135	5	9	2.0447	1.7885	0.9294	1.5281
GPS	2023-11-04	00:00:01	-2267749.26211	5009153.65962	3221293.27026	30.5317	114.3573	26.6135	5	9	2.0449	1.7886	0.9294	1.5282
GPS	2023-11-04	00:00:02	-2267749.17018	5009153.07485	3221293.15356	30.5317	114.3573	26.6267	5	9	2.0450	1.7888	0.9295	1.5283
GPS	2023-11-04	00:00:03	-2267749.51515	5009153.29761	3221293.22164	30.5317	114.3573	26.3947	5	9	2.0452	1.7889	0.9295	1.5284
GPS	2023-11-04	00:00:04	-2267748.68768	5009152.79494	3221293.36404	30.5317	114.3573	25.7786	5	9	2.0453	1.7890	0.9295	1.5286
GPS	2023-11-04	00:00:05	-2267749.32598	5009153.33235	3221293.30720	30.5317	114.3573	26.3982	5	9	2.0455	1.7891	0.9296	1.5287
GPS	2023-11-04	00:00:06	-2267749.45174	5009153.34574	3221293.68953	30.5317	114.3573	26.6476	5	9	2.0456	1.7893	0.9296	1.5288
GPS	2023-11-04	00:00:07	-2267749.17697	5009153.29818	3221293.53853	30.5317	114.3573	26.4359	5	9	2.0458	1.7894	0.9296	1.5289
GPS	2023-11-04	00:00:08	-2267748.93018	5009152.98672	3221293.44027	30.5317	114.3573	26.0540	5	9	2.0459	1.7895	0.9297	1.5291
GPS	2023-11-04	00:00:09	-2267749.15025	5009152.75025	3221293.52871	30.5317	114.3573	25.9915	5	9	2.0461	1.7896	0.9297	1.5292
GPS	2023-11-04	00:00:10	-2267749.15683	5009153.04428	3221293.45143	30.5317	114.3573	26.1853	5	9	2.0462	1.7897	0.9297	1.5293
GPS	2023-11-04	00:00:11	-2267748.95788	5009152.77546	3221293.53700	30.5317	114.3573	25.9472	5	9	2.0464	1.7899	0.9298	1.5294
GPS	2023-11-04	00:00:12	-2267748.82219	5009152.67861	3221293.47941	30.5317	114.3573	25.7937	5	9	2.0465	1.7900	0.9298	1.5296
GPS	2023-11-04	00:00:13	-2267749.07102	5009152.83847	3221293.35878	30.5317	114.3573	25.9463	5	9	2.0466	1.7901	0.9298	1.5297
GPS	2023-11-04	00:00:14	-2267749.18151	5009152.93280	3221293.51178	30.5317	114.3573	26.1273	5	9	2.0468	1.7902	0.9299	1.5298
GPS	2023-11-04	00:00:15	-2267748.86912	5009152.69634	3221293.26282	30.5317	114.3573	25.7143	5	9	2.0469	1.7904	0.9299	1.5299
GPS	2023-11-04	00:00:16	-2267749.46516	5009152.88622	3221293.58354	30.5317	114.3573	26.2379	5	9	2.0471	1.7905	0.9299	1.5300
GPS	2023-11-04	00:00:17	-2267749.02148	5009152.27774	3221293.53364	30.5317	114.3573	25.5646	5	9	2.0472	1.7906	0.9300	1.5302
GPS	2023-11-04	00:00:18	-2267749.36618	5009152.60241	3221293.33147	30.5317	114.3573	26.0090	5	9	2.0474	1.7907	0.9300	1.5303
GPS	2023-11-04	00:00:19	-2267748.01764	5009152.58405	3221293.54522	30.5317	114.3573	25.8270	5	9	2.0475	1.7909	0.9300	1.5304
GPS	2023-11-04	00:00:20	-2267748.97954	5009152.80294	3221293.35676	30.5317	114.3573	25.8849	5	9	2.0477	1.7910	0.9301	1.5305
GPS	2023-11-04	00:00:21	-2267749.25607	5009153.13238	3221293.55336	30.5317	114.3573	26.3415	5	9	2.0478	1.7911	0.9301	1.5307
GPS	2023-11-04	00:00:22	-2267748.64809	5009153.39794	3221293.63188	30.5317	114.3573	26.7290	5	9	2.0479	1.7912	0.9301	1.5308
GPS	2023-11-04	00:00:23	-2267748.67438	5009151.99822	3221293.50875	30.5317	114.3573	25.0082	5	9	2.0481	1.7913	0.9302	1.5309
GPS	2023-11-04	00:00:24	-2267748.94756	5009152.60471	3221293.31799	30.5317	114.3573	25.6983	5	9	2.0482	1.7915	0.9302	1.5310
GPS	2023-11-04	00:00:25	-2267748.02148	5009152.61481	3221293.51865	30.5317	114.3573	25.5646	5	9	2.0484	1.7916	0.9302	1.5312
GPS	2023-11-04	00:00:26	-2267748.97111	5009152.49577	3221293.01029	30.5317	114.3573	25.4649	5	9	2.0485	1.7917	0.9303	1.5313
GPS	2023-11-04	00:00:27	-2267749.24179	5009152.78111	3221293.33332	30.5317	114.3573	25.9490	5	9	2.0487	1.7918	0.9303	1.5314
GPS	2023-11-04	00:00:28	-2267749.37222	5009153.07329	3221293.53348	30.5317	114.3573	26.3263	5	9	2.0488	1.7920	0.9303	1.5315
GPS	2023-11-04	00:00:29	-2267749.25607	5009153.13238	3221293.55336	30.5317	114.3573	25.7080	5	9	2.0489	1.7921	0.9304	1.5316
GPS	2023-11-04	00:00:30	-2267748.63360	5009153.29210	3221293.49942	30.5317	114.3573	26.5735	5	9	2.0491	1.7922	0.9304	1.5317
GPS	2023-11-04	00:00:31	-2267749.37036	5009153.00668	3221293.50387	30.5317	114.3573	26.2536	5	9	2.0492	1.7923	0.9304	1.5318
GPS	2023-11-04	00:00:32	-2267749.46107	5009153.93674	3221293.72095	30.5317	114.3573	26.3460	5	9	2.0494	1.7924	0.9305	1.5320
GPS	2023-11-04	00:00:33	-2267749.58128	5009153.00174	3221293.33654	30.5317	114.3573	26.2444	5	9	2.0495	1.7926	0.9305	1.5321
GPS	2023-11-04	00:00:34	-2267749.30319	5009152.83344	3221293.40281	30.5317	114.3573	26.0472	5	9	2.0497	1.7927	0.9305	1.5323
GPS	2023-11-04	00:00:35	-2267749.92915	5009152.24940	3221293.38263	30.5317	114.3573	25.4458	5	9	2.0498	1.7928	0.9306	1.5324
GPS	2023-11-04	00:00:36	-2267749.47155	5009152.72181	3221293.44931	30.5317	114.3573	26.0476	5	9	2.0500	1.7929	0.9306	1.5325
GPS	2023-11-04	00:00:37	-2267749.84352	5009151.85083	3221293.30280	30.5317	114.3573	25.0113	5	9	2.0502	1.7930	0.9307	1.5326
GPS	2023-11-04	00:00:38	-2267749.16653	5009152.83833	3221293.38397	30.5317	114.3573	25.6084	5	9	2.0504	1.7932	0.9307	1.5327
GPS	2023-11-04	00:00:39	-2267749.84827	5009152.63374	3221293.17151	30.5317	114.3573	25.2085	5	9	2.0505	1.7934	0.9307	1.5328
GPS	2023-11-04	00:00:40	-2267749.03898	5009152.03374	3221293.17151	30.5317	114.3573	24.8934	5	9	2.0507	1.7935	0.9308	1.5329
GPS	2023-11-04	00:00:42	-2267749.03015	5009152.34172	3221293.44892	30.5317	114.3573	25.5878	5	9	2.0508	1.7937	0.9308	1.5332
GPS	2023-11-04	00:00:43	-2267749.12448	5009152.18779	3221293.32334	30.5317	114.3573	25.4367	5	9	2.0510	1.7938	0.9308	1.5333
GPS	2023-11-04	00:00:44	-2267748.65241	5009151.65980	3221293.00595	30.5317	114.3573	24.6935	5	9	2.0511	1.7939	0.9309	1.5335
GPS	2023-11-04	00:00:45	-2267748.75000	5009151.74094	3221293.14580	30.5317	114.3573	24.8628	5	9	2.0512	1.7940	0.9309	1.5336

Fig. 12 position information file

Date	Time	G05	G11	G13	G15	G18	G20	G23	G24	G29	G30	R01	R07	R08	R09
2023-11-04	00:00:01	42.073	129.352	44.613	255.263	319.359	77.203	284.791	173.686	249.590	48.522	265.087	36.828	353.541	nan
2023-11-04	00:00:02	42.094	129.362	44.597	255.300	319.361	77.217	284.803	173.681	249.569	48.510	265.109	36.838	353.565	nan
2023-11-04	00:00:03	42.105	129.367	44.589	255.319	319.362	77.224	284.809	173.678	249.559	48.505	265.120	36.844	353.577	nan
2023-11-04	00:00:04	42.116	129.372	44.581	255.338	319.363	77.231	284.816	173.675	249.548	48.499	265.131	36.849	353.590	nan
2023-11-04	00:00:05	42.127	129.377	44.574	255.357	319.364	77.238	284.822	173.672	249.538	48.493	265.142	36.854	353.602	nan
2023-11-04	00:00:06	42.138	129.382	44.561	255.375	319.365	77.246	284.824	173.669	249.527	48.476	265.152	36.858	353.614	nan
2023-11-04	00:00:07	42.149	129.387	44.558	255.395	319.367	77.253	284.834	173.666	249.517	48.482	265.163	36.865	353.627	nan
2023-11-04	00:00:08	42.159	129.392	44.555	255.414	319.368	77.260	284.840	173.664	249.507	48.476	265.174	36.870	353.639	nan
2023-11-04	00:00:09	42.170	129.397	44.542	255.433	319.369	77.267	284.846	173.661	249.496	48.470	265.185	36.875	353.651	nan
2023-11-04	00:00:10	42.181	129.402	44.534	255.452	319.370	77.274	284.852	173.658	249.486	48.465	265.196	36.880	353.664	nan
2023-11-04	00:00:11</td														

GNSSx	Date	Time	G05	G11	G13	G15	G18	G20	G23	G24	G29	G30	R01	R07	R08	R09
CNRS1	2023-11-04	00:00:00	45.1	33.7	48.9	47.5	36.7	40.8	nan	39.3	46.4	33.1	44.7	40.6	48.0	nan
CNRS1	2023-11-04	00:00:01	45.1	33.6	49.1	47.5	36.7	40.9	nan	39.3	46.3	32.9	44.5	40.6	47.9	nan
CNRS1	2023-11-04	00:00:02	45.0	33.7	49.0	47.5	36.4	40.9	nan	39.3	46.4	33.2	44.7	40.7	47.9	nan
CNRS1	2023-11-04	00:00:03	45.0	33.8	49.0	47.4	36.5	41.0	nan	39.3	46.3	32.8	44.6	40.7	48.0	nan
CNRS1	2023-11-04	00:00:04	45.0	33.8	48.9	47.4	36.5	41.0	nan	39.3	46.3	32.6	44.8	40.7	48.0	nan
CNRS1	2023-11-04	00:00:05	45.0	34.1	48.9	47.3	36.5	40.9	nan	39.4	46.3	33.0	44.8	40.7	47.9	nan
CNRS1	2023-11-04	00:00:06	45.3	34.2	49.0	47.3	36.4	40.9	nan	39.6	46.3	32.6	44.7	40.7	48.0	nan
CNRS1	2023-11-04	00:00:07	45.4	34.3	48.9	47.3	36.5	40.9	nan	39.6	46.4	32.4	44.7	40.6	47.9	nan
CNRS1	2023-11-04	00:00:08	45.3	34.5	48.9	47.4	36.7	41.0	nan	39.5	46.4	32.0	44.6	40.7	47.7	nan
CNRS1	2023-11-04	00:00:09	45.1	34.4	48.9	47.4	36.4	40.7	nan	39.6	46.4	31.6	44.6	40.6	47.7	nan
CNRS1	2023-11-04	00:00:10	44.9	34.7	48.8	47.4	36.7	40.8	nan	39.7	46.4	31.4	44.6	40.4	47.7	nan
CNRS1	2023-11-04	00:00:11	44.8	34.7	48.8	47.3	36.6	40.7	nan	39.8	46.5	31.6	44.5	40.5	47.8	nan
CNRS1	2023-11-04	00:00:12	44.7	34.8	48.8	47.5	37.0	40.6	nan	39.8	46.6	31.1	44.6	40.5	47.6	nan
CNRS1	2023-11-04	00:00:13	44.8	34.8	48.9	47.5	36.8	40.6	nan	39.6	46.6	31.3	44.8	40.4	47.6	nan
CNRS1	2023-11-04	00:00:14	44.5	34.8	48.9	47.6	36.7	40.4	nan	39.6	46.6	31.2	44.7	40.4	47.6	nan
CNRS1	2023-11-04	00:00:15	44.3	34.8	48.9	47.6	36.6	40.4	nan	39.6	46.7	31.1	44.7	40.4	47.5	nan
CNRS1	2023-11-04	00:00:16	44.3	34.8	48.8	47.6	36.7	40.3	nan	39.5	46.8	31.3	44.7	40.3	47.4	nan
CNRS1	2023-11-04	00:00:17	44.1	34.8	48.7	47.6	36.9	40.2	nan	39.4	46.9	31.0	44.7	40.3	47.5	nan
CNRS1	2023-11-04	00:00:18	44.0	34.6	48.7	47.5	36.8	40.1	nan	39.4	46.9	31.2	44.7	40.4	47.4	nan
CNRS1	2023-11-04	00:00:19	43.9	34.8	48.6	47.5	36.8	40.2	nan	39.4	47.0	31.5	44.7	40.5	47.3	nan
CNRS1	2023-11-04	00:00:20	44.0	34.6	48.5	47.5	36.7	40.1	nan	39.4	47.0	31.6	44.7	40.4	47.3	nan
CNRS1	2023-11-04	00:00:21	44.0	34.8	48.6	47.5	36.7	40.1	nan	39.5	46.9	32.0	44.8	40.3	47.3	nan
CNRS1	2023-11-04	00:00:22	43.9	34.4	48.6	47.7	36.3	40.0	nan	39.4	46.8	31.9	44.8	40.4	47.2	nan
CNRS1	2023-11-04	00:00:23	43.9	34.3	48.7	47.7	36.5	39.9	nan	39.3	46.7	32.3	44.7	40.5	47.2	nan
CNRS1	2023-11-04	00:00:24	43.8	34.4	48.7	47.7	36.5	39.9	nan	39.2	46.6	32.3	44.7	40.5	47.1	nan
CNRS1	2023-11-04	00:00:25	43.6	34.1	48.7	47.7	36.5	40.1	nan	39.2	46.7	32.2	44.8	40.4	47.2	nan
CNRS1	2023-11-04	00:00:26	43.5	34.0	48.6	47.9	36.5	39.9	nan	39.0	46.7	32.2	44.8	40.3	47.2	nan
CNRS1	2023-11-04	00:00:27	43.5	34.1	48.6	47.9	36.7	39.9	nan	39.0	46.6	32.7	44.8	40.3	47.2	nan
CNRS1	2023-11-04	00:00:28	43.5	33.9	48.6	47.8	36.8	39.9	nan	39.1	46.7	32.4	45.0	40.0	47.2	nan
CNRS1	2023-11-04	00:00:29	43.5	34.2	48.5	47.9	36.4	39.9	nan	39.2	46.6	32.5	44.8	40.0	47.1	nan
CNRS1	2023-11-04	00:00:30	43.6	34.0	48.6	47.8	36.7	39.8	nan	39.0	46.7	32.5	44.8	39.8	47.1	nan
CNRS1	2023-11-04	00:00:31	43.6	34.0	48.4	47.7	36.6	39.7	nan	38.8	46.6	32.1	44.8	39.9	47.2	nan
CNRS1	2023-11-04	00:00:32	43.6	33.8	48.3	47.7	36.8	39.4	nan	38.9	46.6	32.1	44.8	39.7	47.3	nan
CNRS1	2023-11-04	00:00:33	43.6	33.6	48.4	47.8	36.9	39.4	nan	39.2	46.5	31.7	44.8	39.8	47.3	nan
CNRS1	2023-11-04	00:00:34	43.6	33.8	48.3	47.7	36.8	39.5	nan	39.1	46.3	31.5	44.8	39.7	47.2	nan
CNRS1	2023-11-04	00:00:35	43.6	34.0	48.3	47.6	36.6	39.6	nan	39.1	46.2	31.0	44.8	39.8	47.3	nan
CNRS1	2023-11-04	00:00:36	43.4	33.9	48.3	47.5	36.5	39.7	nan	39.2	46.1	30.9	44.7	39.5	47.2	nan
CNRS1	2023-11-04	00:00:37	43.3	33.7	48.3	47.3	36.6	39.5	nan	39.2	46.0	30.6	44.7	39.5	47.2	nan
CNRS1	2023-11-04	00:00:38	43.3	33.9	48.1	47.2	36.4	39.5	nan	39.2	45.9	30.4	44.7	39.6	47.3	nan
CNRS1	2023-11-04	00:00:39	43.3	33.7	48.1	47.1	36.6	39.3	nan	39.4	45.8	30.4	44.7	39.6	47.3	nan
CNRS1	2023-11-04	00:00:40	43.4	33.8	48.2	47.0	36.6	39.2	nan	39.5	45.8	30.0	44.7	39.6	47.4	nan
CNRS1	2023-11-04	00:00:41	43.6	33.9	48.2	46.9	36.5	39.4	nan	39.4	45.9	29.3	44.7	39.8	47.4	nan
CNRS1	2023-11-04	00:00:42	43.5	33.6	48.3	47.0	36.3	39.5	nan	39.3	45.9	29.4	44.6	39.7	47.4	nan
CNRS1	2023-11-04	00:00:43	43.6	33.5	48.2	47.0	36.6	39.6	nan	39.7	45.9	29.3	44.6	39.7	47.4	nan
CNRS1	2023-11-04	00:00:44	43.9	33.2	48.1	46.9	36.4	39.5	nan	39.5	45.9	29.4	44.6	39.7	47.5	nan
CNRS1	2023-11-04	00:00:45	44.0	33.6	48.2	46.9	36.6	39.5	nan	39.5	45.9	29.8	44.6	39.7	47.6	nan

Fig. 14 C/N0 file

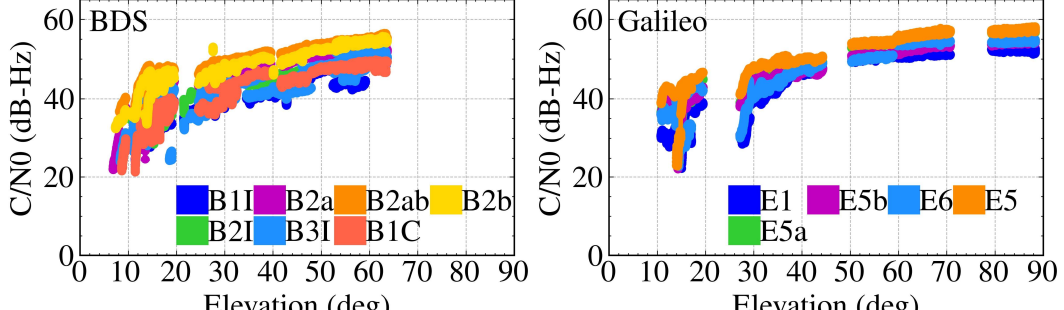


Fig. 15 Carrier-to-noise ratio at different frequencies for two systems

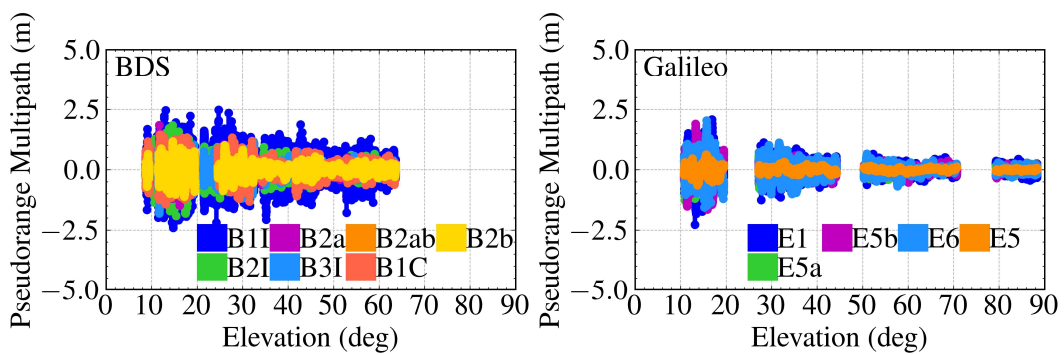


Fig. 16 Pseudorange multipath variation at different frequencies for two systems

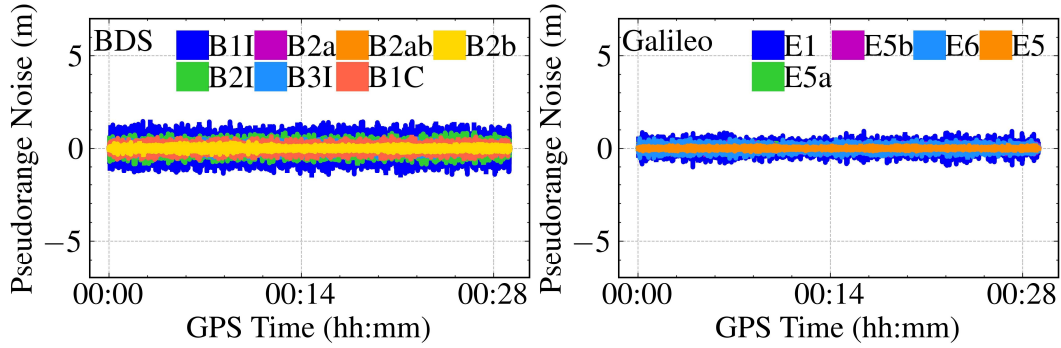


Fig. 17 Pseudorange observation noise sequences at different frequencies for two systems

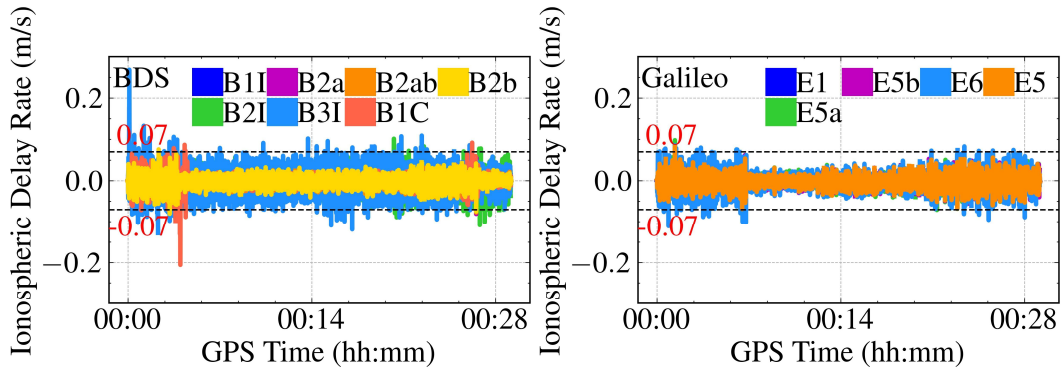


Fig. 18 Ionospheric delay rate at different frequencies for two systems

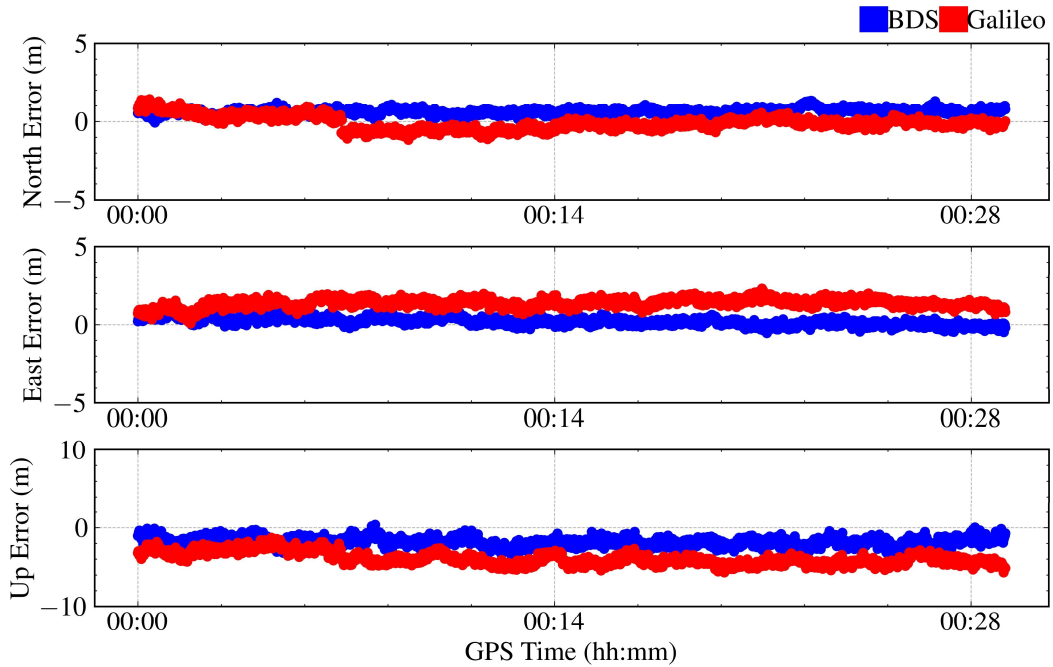


Fig. 19 Single point positioning results for two systems

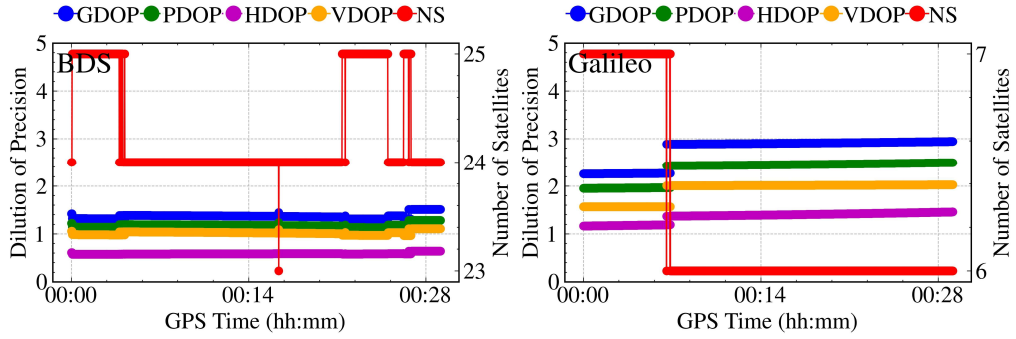


Fig. 20 Number of visible satellites and DOP for two systems

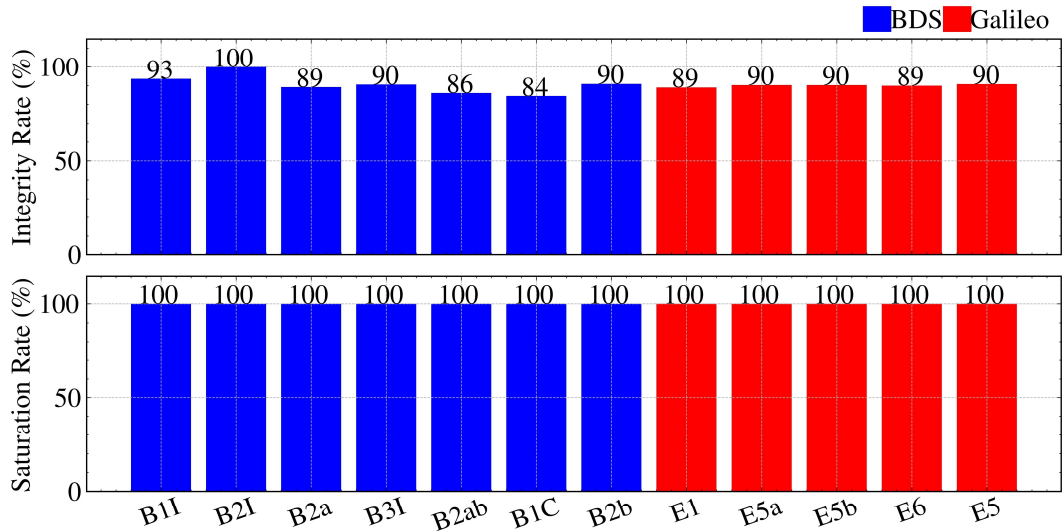


Fig. 21 Statistics result of data integrity and saturation rate for two systems

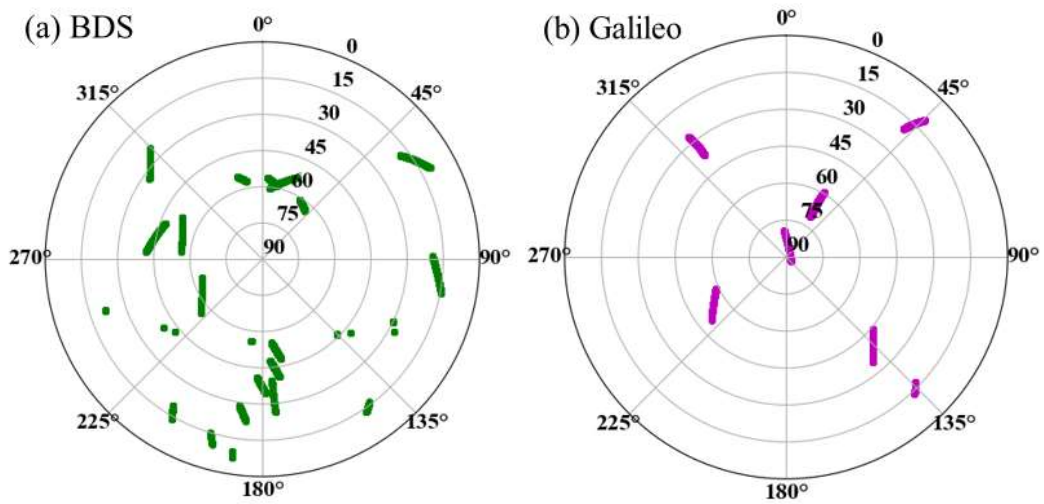


Fig. 22 Sky view of all satellites for two systems

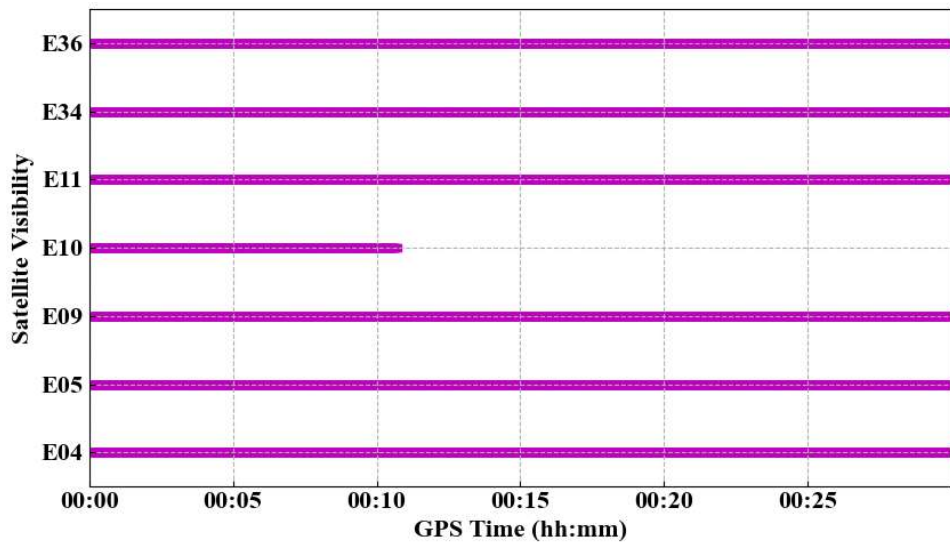
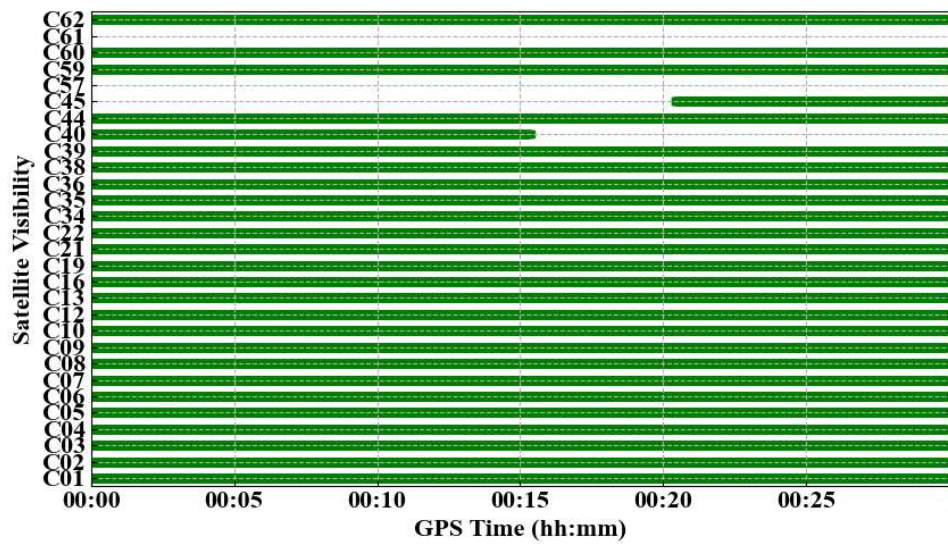


Fig. 23 Observation sequences of all satellites for two systems

6 Mathematical methods

The basic undifferenced observations of the original pseudorange and phase can be given as follows:

$$\begin{cases} P_{r,i}^s = \rho_r^s + c(\delta t_r - \delta t^s) + \gamma_i^s I_{r,i}^s + Mw_i^s \cdot ZWD_r + c(b_{r,i}^s - b_i^s) + \xi_{r,i}^s \\ L_{r,i}^s = \rho_r^s + c(\delta t_r - \delta t^s) - \gamma_i^s I_{r,i}^s + Mw_i^s \cdot ZWD_r + \lambda_i^s N_{r,i}^s + c(B_{r,i}^s + B_i^s) + \zeta_{r,i}^s \end{cases} \quad (1)$$

where s denotes a specific satellite; r denotes receiver; ρ_r^s denotes the satellite-to-receiver range (m); c denotes light velocity (m/s); δt_r and δt^s denote receiver and satellite clock offsets (s), respectively; Mw_r^s and ZWD_r denote the wet mapping function and the zenith troposphere wet delay, respectively; γ_i^s denotes the frequency correlation coefficient ($\gamma_i^s = (f_1)^2 / (f_i)^2$); $I_{r,i}^s$ denotes the slant ionospheric delay (m); λ_i^s and $N_{r,i}^s$ denote the wavelength and the integer phase ambiguity, respectively; $b_{r,i}^s$ and b_i^s denote the frequency-dependent receiver and satellite code biases, respectively (s); $B_{r,i}^s$ and B_i^s denote the frequency-dependent receiver and satellite phase biases, respectively (s); $\xi_{r,i}^s$ and $\zeta_{r,i}^s$ denote the sum of measurement noise and other unmodeled error for pseudorange and phase observations, respectively.

6.1 Pseudorange gross error detection

The commonly used pseudorange observations are P_1 , P_2 , and C_1 codes. By using differential methods, then construct the following pseudorange gross error test quantity:

$$dC_1P_1 = C_1 - P_1 = DCB_{C_1P_1}^s + DCB_{r,C_1P_1} + S_{C_1-P_1} + \varepsilon_{C_1-P_1} \quad (2)$$

$$dP_1P_2 = P_1 - P_2 = DCB_{P_1P_2}^s + DCB_{r,P_1P_2} + S_{P_1-P_2} + d_{ion} + \varepsilon_{P_1-P_2} \quad (3)$$

where $DCB_{C_1P_1}^s$, $DCB_{P_1P_2}^s$, DCB_{r,C_1P_1} and DCB_{r,P_1P_2} denote the receiver and satellite differential code bias, respectively; $S_{C_1-P_1}$ and $S_{P_1-P_2}$ denote the time variable of differential code bias; d_{ion} denotes the ionospheric delay residual error term between two frequencies; $\varepsilon_{C_1-P_1}$ and $\varepsilon_{P_1-P_2}$ denote the remaining error of combination. The combined detection quantity of dC_1P_1 and dP_1P_2 is detected:

$$\begin{cases} H_0 : \text{normal} & |dC_1P_1| \leq k_1 \text{ and } |dP_1P_2| \leq k_2 \\ H_1 : \text{abnormality} & |dC_1P_1| > k_1 \text{ and } |dP_1P_2| > k_2 \end{cases} \quad (4)$$

where k_1 and k_2 denote the test threshold. Generally, k_1 and k_2 are 30m and 60m.

6.2 Cycle slip detection

6.2.1 MW combination

The Melbourne-Wunnema (MW) combination is the difference between the wide-lane phase and narrow-lane pseudorange combination, and its expression is:

$$L_{MW} = \lambda_w N_w = \frac{f_i L_{r,i}^s - f_j L_{r,j}^s}{f_i - f_j} - \frac{f_i P_{r,i}^s + f_j P_{r,j}^s}{f_i + f_j} \quad (5)$$

where f_i^s and f_j^s denote the signal frequency; λ_w denote $\lambda_w = c / (f_i - f_j)$.

When there is no cycle slip, the value of N_w has no significant difference. Therefore, the

cycle slip test quantity is constructed as follows:

$$N_w = \frac{L_{MW}}{\lambda_w} \quad (6)$$

The average wide-lane ambiguity and root mean square at each epoch are calculated according to the recursive formula:

$$\bar{N}_w(i) = \bar{N}_w(i-1) + \frac{1}{i} [N_w(i) - \bar{N}_w(i-1)] \quad (7)$$

$$\sigma^2(i) = \sigma^2(i-1) + \frac{1}{i} [(N_w(i) - \bar{N}_w(i-1))^2 - \sigma^2(i-1)] \quad (8)$$

where $\bar{N}_w(i)$ denotes the average value of wide lane ambiguity; $\sigma^2(i)$ denotes the variance.

If Eq. (9) is satisfied, cycle slips occur; gross errors occur if Eq. (10) is satisfied. Take the previous $i-1$ epochs as a segment, record its value of $\bar{N}_w(i-1)$ and variance of $\sigma(i-1)$ for subsequent processing, and divide it into a new segment from the epoch i .

$$\left. \begin{array}{l} |N_w(i) - \bar{N}_w(i-1)| \geq 4\sigma(i-1) \\ |N_w(i) - N_w(i+1)| \leq 1 \end{array} \right\} \quad (9)$$

$$\left. \begin{array}{l} |N_w(i) - \bar{N}_w(i-1)| \geq 4\sigma(i-1) \\ |N_w(i) - N_w(i+1)| > 1 \end{array} \right\} \quad (10)$$

6.2.2 GF combination

The linear combination of Geometry-Free (GF) is defined by the following equation:

$$GF_{r,jj}^s = L_{r,i}^s - L_{r,j}^s = \lambda_r^s N_{r,i}^s - \lambda_r^s N_{r,j}^s - \gamma_i^s I_{r,i}^s + \gamma_j^s I_{r,j}^s + e \quad (11)$$

where e denotes the carrier phase combination observation noise. The detection expression is as follows:

$$|GF_{r,jj}^s(t) - GF_{r,jj}^s(t-1)| > k\sigma_{GF} + \Delta I_{\max} \quad (12)$$

where k denotes 4; ΔI_{\max} denotes 0.4m/h.

6.3 Clock jump detection and repair

The deviation between the receiver and the satellite clock accumulates over time. To maintain synchronization, it is necessary to insert clock jumps into the receiver clock. Therefore, it is essential to detect and repair clock jumps by using the difference method between adjacent observation epochs:

$$\left. \begin{array}{l} \Delta P_{r,i}^s(t) = P_{r,i}^s(t) - P_{r,i}^s(t-1) \\ \Delta L_{r,i}^s(t) = L_{r,i}^s(t) - L_{r,i}^s(t-1) \end{array} \right\} \quad (13)$$

where t denotes epoch. Construct the detection quantity and its conditional equation:

$$\left. \begin{array}{l} T^s(t) = \Delta P_{r,i}^s(t) - \Delta L_{r,i}^s(t) \\ |T^s(t)| > k_1 \approx 0.001 \cdot c \end{array} \right\} \quad (14)$$

where k_1 denotes the detection threshold. For epoch t , only when all satellites satisfy the test condition Eq. (14), it is considered that the clock jump occurs in this epoch or all satellites have a large cycle slip, then use Eq. (15) to calculate the clock jump candidate, and Eq. (16) to determine the actual clock jump J .

$$m = \alpha \cdot \left(\sum_{s=1}^n T^s \right) / (n \cdot c) \quad (15)$$

$$J = \begin{cases} \text{int}(m), & |m - \text{int}(m)| \leq k_2 \\ 0, & |m - \text{int}(m)| > k_2 \end{cases} \quad (16)$$

where α denotes the coefficient factor; k_2 denotes the threshold.

After detecting and calculating J , the clock jump can be repaired in reverse. The corresponding calculation expression is:

$$GF_{r,j}^s(t) - GF_{r,j}^s(t-1) > k\sigma_{GF} + \Delta_{\max} \tilde{L}_{r,i}^s(t) = L_{r,i}^s(t) + J \cdot c / \alpha \quad (17)$$

where $\tilde{L}_{r,i}^s(t)$ denotes the observations of the repaired carrier phase.

6.4 Data integrity rate

The data integrity rate is one of the essential indicators to measure the availability and completeness of receiver observation files. It mainly tests the number of lost observation epochs, reflecting the performance of receiver data reception and the impact of the surrounding environment on data reception. The data integrity rate is the ratio of actual epoch numbers with pseudorange and carrier phase values at the i frequency of satellite s to the theoretical number. Its expression is:

$$\text{ratio} = \sum_{s=1}^n N_{i,R}^s / \sum_{s=1}^n N_{i,T}^s \quad (18)$$

where n denotes the number of all visible satellites within a certain period of time; $N_{i,R}^s$ and $N_{i,T}^s$ denote the actual received data and the theoretical received data, respectively.

6.5 Data saturation rate

The data saturation rate is the minimum to maximum data amount ratio in different data types (pseudorange and carrier phase observations). Its expression is:

$$\kappa = \min(N_{i,PL}^s) / \max(N_{i,PL}^s) \quad (19)$$

where $N_{i,PL}^s$ denotes the number of observations of various types on the i frequency of satellite s .

6.6 Pseudorange multipath

Pseudorange multipath is related to the station environment. When dual-frequency observations are available, a combination of single-frequency pseudorange and dual-frequency carrier phase observations calculates pseudorange multipath as follows:

$$\begin{cases} PMP_{r,i}^s = P_{r,i}^s - \frac{f_i^2 + f_j^2}{f_i^2 - f_j^2} L_{r,i}^s + \frac{2f_j^2}{f_i^2 - f_j^2} L_{r,j}^s \\ PMP_{r,j}^s = P_{r,j}^s - \frac{2f_i^2}{f_i^2 - f_j^2} L_{r,i}^s + \frac{f_i^2 + f_j^2}{f_i^2 - f_j^2} L_{r,j}^s \end{cases} \quad (20)$$

where $PMP_{r,i}^s$ and $PMP_{r,j}^s$ denote the computational amount including multipath error and integer ambiguity on the i and j frequencies, respectively.

For the epoch intervals with continuous observation and no cycle slips, the integer ambiguity is a constant, and the pseudorange multipath error can be calculated by Eq. (21).

$$\widetilde{PMP}_{r,i}^s = PMP_{r,i}^s - \langle PMP_{r,i}^s \rangle \quad (21)$$

where $\langle \cdot \rangle$ denotes smoothing in the time domain.

6.7 Carrier phase multipath

Some satellite systems provide three-frequency and above carrier phase observations, using two dual-frequency ionosphere-free combinations to calculate carrier phase multipath; the corresponding expression is:

$$\begin{aligned} LMP_r^s(L_{r,i}^s, L_{r,j}^s, L_{r,k}^s) &= IF(L_{r,i}^s, L_{r,j}^s) - IF(L_{r,i}^s, L_{r,k}^s) \\ &= \left(\frac{f_i^2}{f_i^2 - f_j^2} - \frac{f_i^2}{f_i^2 - f_k^2} \right) \cdot L_{r,i}^s - \frac{f_j^2}{f_i^2 - f_j^2} \cdot L_{r,j}^s + \frac{f_k^2}{f_i^2 - f_k^2} \cdot L_{r,k}^s \end{aligned} \quad (22)$$

6.8 Ionospheric delay rate

The ionospheric delay rate refers to the change in ionospheric delay per unit of time. When dual-frequency observations are available, the ionospheric delay rate can be calculated by using the difference method between adjacent epochs expressed as follows:

$$\begin{cases} I_i = \frac{f_j^2}{f_i^2 - f_j^2} (L_{r,i}^s - L_{r,j}^s) \\ I_j = \frac{f_i^2}{f_i^2 - f_j^2} (L_{r,i}^s - L_{r,j}^s) \end{cases} \quad (23)$$

$$\begin{cases} IOD_i = \frac{I_i(t_k) - I_i(t_{k-1})}{t_k - t_{k-1}} \\ IOD_j = \frac{I_j(t_k) - I_j(t_{k-1})}{t_k - t_{k-1}} \end{cases} \quad (24)$$

where IOD_i and IOD_j denote the ionosphere delay rate on the i and j frequencies, respectively.

6.9 Carrier-to-noise ratio

The carrier-to-noise ratio value (C/N_0) is the ratio between signal strength and noise. It is mainly affected by the antenna gain parameter, the state of the correlator in the receiver, and the multipath effect. C/N_0 can be obtained directly from the station's original observation data. The lower the value of C/N_0 , the higher the noise intensity and the worse the signal quality.

6.10 Pseudorange observation noise

Pseudorange observation noise not only reflects the quality of the satellite signal but also reflects the overall performance of the receiver. The pseudorange noise is calculated using the difference method between adjacent epochs, and its expression is:

$$\Delta P_{r,i}^s(t_k) = P_{r,i}^s(t_k) - 3P_{r,i}^s(t_{k-1}) + 3P_{r,i}^s(t_{k-2}) - P_{r,i}^s(t_{k-3}) \quad (25)$$

$$\bar{\sigma}_P = \frac{1}{n} \times \sum_{j=1}^n \sqrt{\frac{1}{20 \times N} \sum_{k=1}^N [\Delta P_{r,i}^j(k)]^2} \quad (26)$$

where n denotes the number of satellites; N denotes the number of observations; $\bar{\sigma}_P$ denotes the estimation of pseudorange observation noise.

6.11 Carrier phase observation noise

Similar to pseudorange noise calculation, the carrier phase noise is calculated using the difference method between adjacent epochs, and its expression is:

$$\Delta L_{r,i}^s(t_k) = L_{r,i}^s(t_k) - 3L_{r,i}^s(t_{k-1}) + 3L_{r,i}^s(t_{k-2}) - L_{r,i}^s(t_{k-3}) \quad (27)$$

$$\bar{\sigma}_L = \frac{1}{n} \times \sum_{j=1}^n \sqrt{\frac{1}{20 \times N} \sum_{k=1}^N [\Delta L_{r,i}^j(k)]^2} \quad (28)$$

where $\bar{\sigma}_L$ denotes the estimation of carrier phase observation noise.

6.12 Dilution of precision

The Dilution of Precision (DOP) reflects the positioning performance and the satellite's spatial distribution status. The smaller the DOP value, the better the spatial geometric distribution of the observation satellites and the smaller the positioning error, and its expression is:

$$G = \begin{bmatrix} \cos E_1 \sin A_1 & \cos E_1 \cos A_1 & \sin E_1 & 1 \\ \cos E_2 \sin A_2 & \cos E_2 \cos A_2 & \sin E_2 & 1 \\ \vdots & \vdots & \vdots & \vdots \\ \cos E_n \sin A_n & \cos E_n \cos A_n & \sin E_n & 1 \end{bmatrix} \quad (29)$$

$$Q = (G^T G)^{-1} = \begin{bmatrix} q_{XX} & q_{XY} & q_{XZ} & q_{XT} \\ q_{YX} & q_{YY} & q_{YZ} & q_{YT} \\ q_{ZX} & q_{ZY} & q_{ZZ} & q_{ZT} \\ q_{TX} & q_{TY} & q_{TZ} & q_{TT} \end{bmatrix} \quad (30)$$

$$GDOP = \sqrt{q_{XX} + q_{YY} + q_{ZZ} + q_{TT}} \quad (31)$$

$$PDOP = \sqrt{q_{XX} + q_{YY} + q_{ZZ}} \quad (32)$$

where A_i denotes the satellite azimuth; E_i denotes the satellite elevation; n denotes the number of satellites; G denotes observation matrix; Q denotes cofactor matrix; $GDOP$ denotes geometric dilution precision; $PDOP$ denotes position dilution precision.

Acknowledgement

Thank Mr. Tim Everett for the open-source rtklib-py program, which has provided us with reference and inspiration.